Application of eucalyptus wood waste-derived biochar for adsorption of aluminum from aqueous solutions

Yu Shuang Ren[a], Hizbullah Khan[b], Bushra Khan[b], Muhammad Ilyas[b,c,]*, Shahid Iqbal[d]

[a]*School of Economics and Management, Jilin Jianzhu University, Chang Chun 130117, China, email: rysmiracle@126.com*
[b]*Department of Environmental Sciences, University of Peshawar, Peshawar, Khyber Pakhtunkhwa, Pakistan,*
Tel. +923078064028; emails: sirfilyas@yahoo.com (M. Ilyas), hizbullah@uop.edu.pk (H. Khan), bushraasu@yahoo.com (B. Khan)
[c]*Department of Environmental Sciences, Shaheed Benazir Bhutto University Dir Upper Khyber Pakhtunkhwa, Pakistan*
[d]*Centre for Disaster Preparedness and Management, University of Peshawar, Peshawar, Khyber Pakhtunkhwa, Pakistan,*
email: shahidiqbalkhan@uop.edu.pk

ABSTRACT

The current study reports the adsorption of aluminum (Al^{3+}) from aqueous solutions through batch experiments using eucalyptus wood waste-derived biochar (EWB). The EWB morphology and structure were observed by surface area analysis, scanning electron microscopy, as well as Fourier-transform infrared spectroscopy. A thorough analysis of the variables influencing adsorption performance was conducted. The adsorption process was examined using the Freundlich, Langmuir, pseudo-second-order models as well as pseudo-first-order. The EWB showed a high adsorption rate in low concentration Al^{3+} solutions. The adsorption of Al^{3+} was exothermic and spontaneous. The prepared EWB are very promising as an alternative adsorbent for Al^{3+} due to their porous structure and high adsorption capacity (>90%).

Keywords: Adsorptive removal; Kinetics and isotherm; Thermodynamics study; Aqueous solution

1. Introduction

Al^{3+} is the 3rd most prevalent element in the Earth's crust after silicon and oxygen, and is a toxic element that is not essential to the human body [1]. Al^{3+} is also contained in the deposited particulate matter [2]. The excessive use of aluminum salts (alum) in chemical treatment processes in water treatment plants as a coagulant to remove microorganisms, color, turbidity as well as organic matter [3,4]. Al^{3+} can cause neurological disorders, including Alzheimer's disease (AD), amyotrophic lateral sclerosis, as well as Parkinson's dementia [5,6]. The World Health Organization estimates that the number of people infected with the AD disease will reach 9 million by 2030 [1].

In the past few years, a lot of work has been done on the treatment of wastewater. Diverse methods are created to cater the elimination of toxic elements as of wastewater, which incorporate reduction, chemical precipitation, chemical reduction/oxidation, electrochemical treatment, photocatalytic reduction, membrane separation, ion-exchange, coagulation or flocculation, chemical precipitation, complexation, filtrations, electrochemical precipitation, solid phase adsorption, biosorption, as well as adsorption [7–15]. In any case, the majority of these techniques have some impediments, such as high venture and support costs, confused working systems [16].

Adsorption is an important wastewater treatment technique that is widely used to remove toxic metals from wastewater [17,18]. Assortment of adsorbents utilized for this

* Corresponding author.

reason incorporates chemically treated biosorbents [19,20], *Rhizopus oryzae* [21], biochar/bentonite/waste polyethylene terephthalate as well as biochar/bentonite/waste polystyrene [17], *Phoenix dactylifera* coir wastes [22], *Ziziphus* leaf [23], *Moringa oleifera* seed pod [24], microalgae [25], *Sargassum hystrix* algae [26], *Padina sanctae-crucis* algae [27], various other adsorbents [28], biosorbents [29], montmorillonite clay [30], cuttlebone [31], shrimp shell waste [32], green synthesis of silver nanoparticles [33], ligand based composite material [34], metal/mineral-incorporating materials [35], iron oxide-impregnated dextrin nanocomposite [36], ether based mesoporous adsorbent [37], magnetic glycine-modified chitosan [38], papaya peel carbon [39], ligand functionalized organic–inorganic based novel composite [40], thiourea-formaldehyde resin and its magnetic derivative [41], chitosan grafted polyaniline [42], modified conjugate material [43], CuO as well as $Cu(OH)_2$ embedded chitosan [44], waste rubber tires [45], ligand-doped conjugate adsorbent [46], magnetic glycidyl methacrylate resin [47], iron-based metal organic framework [48], novel optical adsorbent [49], ligand-based efficient conjugate nanomaterials [50], and novel facial composite adsorbent [51,52].

In the current research work, the eucalyptus wood waste-derived biochar (EWB) has been prepared successfully by a simple and low-cost method. The adsorption performance of EWB was evaluated by batch experiments, and the adsorption behavior of EWB for Al^{3+} was studied in detail, including the effect of initial Al^{3+} concentration, temperature, contact time, pH, adsorbent dose, adsorption isotherm, and adsorption kinetics, and the research results indicate the remarkable adsorption performance of EWB for Al^{3+} make it has the potential to meet actual application requirements, which has very special significance for pollution control and remediation.

2. Materials and methods

2.1. Chemicals and materials

The University of Agriculture (Peshawar, Pakistan) provided biochar made from eucalyptus wood. All chemicals and reagents were of analytical grade and utilized without further purification, and the water used in this investigation was deionized. $Al(NO_3)_3$ salt was dissolved in 1,000 mL of deionized water to prepare the stock solution of Al^{3+} (1,000 mg/L).

2.2. Synthesis of biochar from eucalyptus wood waste

The process of making biochar from eucalyptus wood waste involved pyrolysis at 450°C for 1 h in a high performance automatic controlled furnace with a continuous nitrogen flow. It was necessary to run the off-gas through a cooling chamber filled with water in order to allow the heavy tar to condense. The EWB was subsequently cooled to room temperature within the furnace while being exposed to nitrogen.

2.3. Characterization of EWB

The Fourier-transform infrared spectroscopy (FTIR) spectra were measured by a Nicolet iS10 FTIR Spectrometer (Cary630, Agilent Technologies, USA) with a scanning range of 4,000–400 cm^{-1}. The scanning electron microscopy (SEM) images were obtained using the FEI Quanta 450 FEG Scanning Electron Microscope (JSM-5910, JEOL, Japan). Furthermore, the Brunauer–Emmet–Teller (BET) data of the samples were tested by a nitrogen adsorption instrument, Autosorb iQ2.

2.4. Adsorption performance test

Add 0.1 g of the dried EWB sample to 100 mL of Al^{3+} solution, and the mixture were shaken for 1 h at 25°C in a thermostatic shaking chamber at 150 rpm. The effects of EWB dosage, initial Al^{3+} concentration, pH, temperature, and contact time on the adsorption efficiency were systematically studied. A flame-moded atomic absorption spectrophotometer (AAnalyst 700, PerkinElmer, USA) was used to measure the amount of Al^{3+} in the adsorption solution. Calculations of the corresponding adsorption capacity (q_e) (mg/g) as well as percent removal (%) of EWB were made using the formulae listed in Table 1 [17].

Different adsorption models, such as Freundlich in addition to Langmuir isotherms, were applied in order to further study the adsorption behaviour (Table 2). By incorporating the adsorption data into the first and second-order kinetic equations (Table 3), the adsorption kinetics was also examined [17]. The effect of temperature on the thermodynamics parameters $\Delta G°$, $\Delta H°$ and $\Delta S°$) was also examined (Table 4) [32–35].

Table 1
Equations used for q_e and % q_e calculations

	Equation	
Equilibrium concentration	$q_e = \dfrac{\left[(C_o - C_i) \times V\right]}{M}$ where,	(1)
	C_o (mg/L) = Initial Al^{3+} concentration; C_i (mg/L) = Equilibrium Al^{3+} concentration; V (L) = Volume of solution; M (g) = Mass of EWB.	
Percentage removal	$\%q_e = \dfrac{\left[(C_o - C_i) \times 100\right]}{C_o}$	(2)

Table 2
Isotherm models used in the study

Model	Equation	
Langmuir	$\dfrac{C_e}{q_e} = \dfrac{1}{KQ_{max}} + \dfrac{C_e}{Q_{max}}$	(3)
	Since, q_e is the quantity of adsorbed Al^{3+} on the eucalyptus wood waste-derived biochar at equilibrium (mg/g) and C_e is the equilibrium-concentration of the Al^{3+} (mg/L).	
Freundlich	$\ln q_e = \ln K_f + \dfrac{1}{n}\ln C_e$	(4)
	Since: n and K_f are the adsorption intensity and capability, respectively.	

Table 3
Kinetic models used in the study

Model	Equation
Pseudo-first-order	$\ln\left(q_e - q_t\right) = \ln q_e + K_{1t}$ (5) Since: q_e and q_t are the amounts of adsorbed Al^{3+} (mg/g) at equilibrium and time t (min), respectively, and K_1 is the rate-constant of pseudo-first-order (min^{-1}).
Pseudo-second-order	$\dfrac{t}{q_t} = \dfrac{t}{q_e} + \dfrac{1}{K_2 q_e^2}$ (6) Since: K_2 is the rate-constant of pseudo-second-order adsorption (g/mg·min) and at equilibrium the sorption capacity is presented by q_e.

Table 4
Equations used for the thermodynamic parameters calculations

Gibbs free energy	$\Delta G° = -RT \ln K_D$ (7) where R is the ideal gas constant, 8.314 J/K·mol⁻¹; T is the absolute temperature in K; K_D is the equilibrium coefficient of the PAHs adsorption on the eucalyptus wood waste-derived biochar.
Enthalpy	$\Delta H° = R \dfrac{T_2 T_1}{T_2 - T_1} \ln \dfrac{K_2}{K_1}$ (8)
Entropy	$\Delta S° = \dfrac{\Delta H° - \Delta G°}{T}$ (9)

3. Results and discussion

3.1. Characterization analysis

SEM, FTIR, and surface area analysis were used to determine the characteristics of the biochars made in the laboratory from eucalyptus wood waste. The granular morphology in the SEM micrograph of EWB (Fig. 1) is non uniform. The biochar particles, which range in size from less than 5 μ to as large as 30 μ, are visible as fine grains and lumps.

The EWB sample FTIR spectrum (Fig. 2) shows peaks centered at around 3,000 and 2,800 cm⁻¹ corresponding to aromatic C–H and methylene C–H bonds. Multiple peaks positioned at 1,630 and 1,500 cm⁻¹ indicates aromatic C=C, a peak around 1,447 cm⁻¹ and 693 indicates methylene C–H vibration.

N_2 adsorption isotherms at 77.35 K (Fig. 3) were used to calculate the surface parameters of the EWB, including pore radius, pore volume, BET surface area (S_{BET}), and Barrett–Joyner–Halenda surface area (S_{BJH}). Table 5 presents the findings. According to the surface analysis results (Table 5), the calculated S_{BJH} for EWB was found to be 14.10 m²/g. The S_{BET} was found to be 18.37 m²/g, with a pore volume of 0.01 cm³/g, and a pore radius of 14.90 A⁰. From the data, it is clear that the EWB adsorbent has high surface area and large pore size. Therefore, EWB has a better adsorption potential.
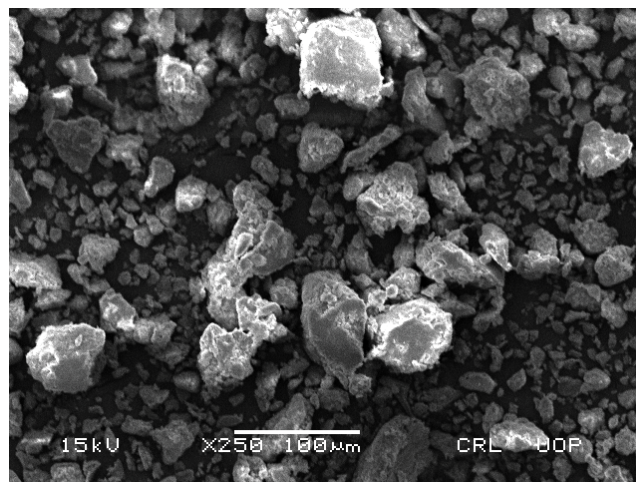

Fig. 1. Scanning electron microscopy image of eucalyptus wood waste-derived biochar.
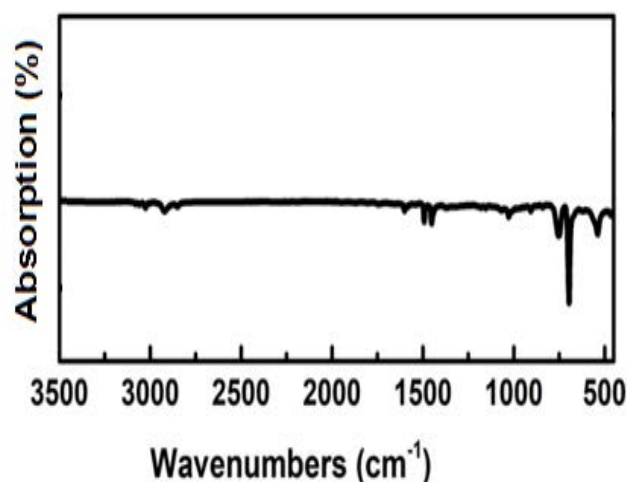

Fig. 2. Fourier-transform infrared spectra of eucalyptus wood waste-derived biochar.
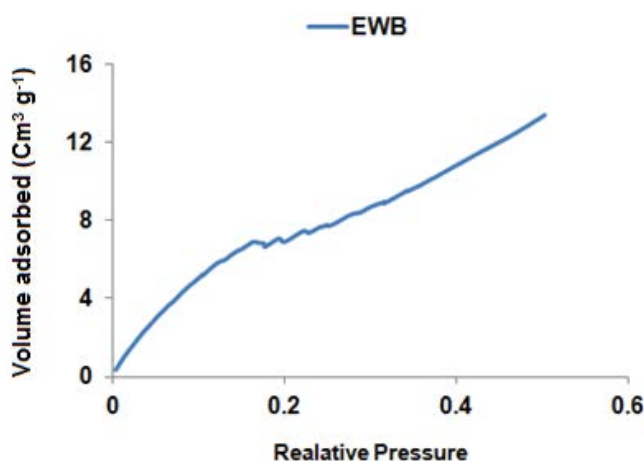

Fig. 3. N_2 adsorption isotherms of eucalyptus wood waste-derived biochar at 77 K.

3.2. Adsorption performance analysis

3.2.1. Effect of contact time

The effect of adsorption time on the amount of Al^{3+} that is adsorbed on the EWB was also studied. The studies were conducted over a range of adsorption durations, including 15, 30, 45, 60, and 90 min. The results are displayed in Fig. 4, which demonstrates that the adsorption of Al^{3+} increases linearly with an increase in adsorption duration and reaches its maximum within 90 min. However, an increase in adsorption beyond this point has no further effect on adsorption. These findings imply that as the adsorption time increases, the number of accessible adsorption sites on the EWB surface initially increases the adsorption rate. The vacancies were filled in less than 90 min, therefore the adsorption stabilised after that [17,53–56]. These findings led to the decision that 90 min was the ideal adsorption time.

3.2.2. Effect of initial Al^{3+} concentration

The impact of the initial Al^{3+} concentration on the EWB adsorption capability is shown in Fig. 5. Adsorption of Al^{3+} was found to be increased when increasing the initial Al^{3+} concentration. This is because of the way that increasing of the initial Al^{3+} concentration may result in the availability of Al^{3+} to adsorb over the adsorbent surface active sites. Similar behavior has been observed in previous studies and arises from the effect of interactions between the initial Al^{3+} concentration and adsorbent [53–56]. Al^{3+} can be effectively adsorbed on the surface of the EWB in low concentrations through hydrogen bonds, hydrophobic and electrostatic interactions, and ion-exchange [17].

3.2.3. Effect of EWB dosage

Another important factor affecting the adsorption level of harmful metals is the amount of adsorbent used. The ability of the adsorbent to be used efficiently while maintaining high adsorption efficiency is typically necessary for the investigation of the optimal adsorbent dosage. The necessary adsorbent dosage was adjusted between 0.1 and 0.3 g/L in order to find the ideal value for Al^{3+} adsorption on EWB. The adsorption effect of EWB adsorbent dose in an aqueous medium is depicted in Fig. 6. As seen in Fig. 6, the adsorption capacity of the adsorbent for Al^{3+} decreases as the adsorption rate rises. This pattern is caused by the dispersion of Al^{3+} over a large fraction of the adsorbent surface area, which reduces the adsorption capacity of EWB per unit mass [17].

3.2.4. Effect of temperature

Temperature is a crucial parameter in adsorption reactions. The Al^{3+} ability to be adsorbed from aqueous solution on the adsorbent will be impacted by temperature changes. Fig. 7 depicts the exothermic nature of the adsorption process of Al^{3+} from aqueous solutions onto EWB at

Table 5
Surface properties of the eucalyptus wood waste-derived biochar

Adsorbent	S_{BJH} (m²/g)	S_{BET} (m²/g)	Pore radius (A^0)	Pore volume (cm³/g)
Eucalyptus wood waste-derived biochar	14.10	18.37	14.90	0.01

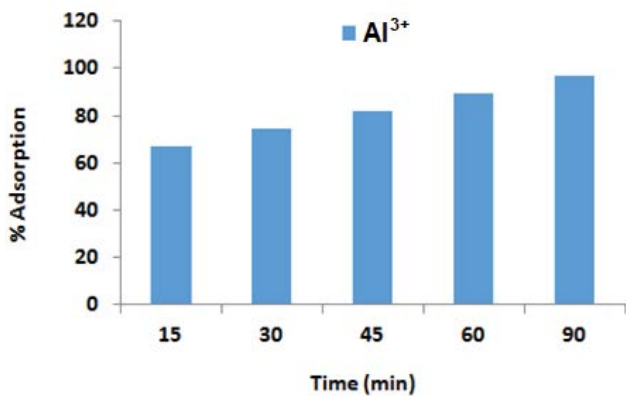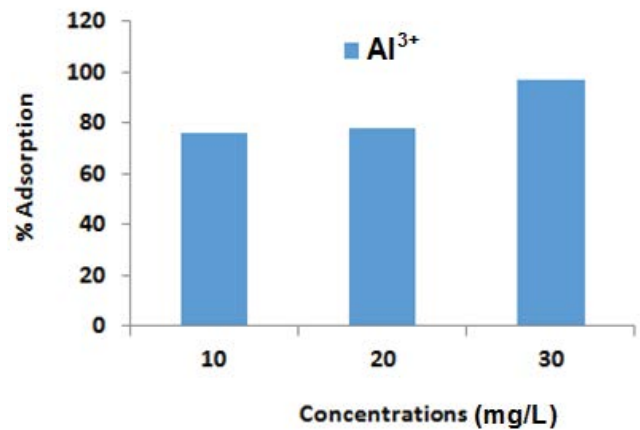Fig. 5. Effect of concentrations on % adsorption of Al^{3+} over eucalyptus wood waste-derived biochar.

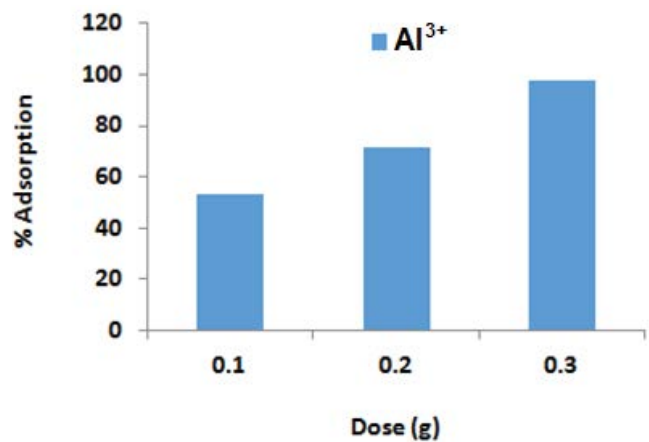Fig. 4. Effect of contact time on % adsorption of Al^{3+} over eucalyptus wood waste-derived biochar.

Fig. 6. Effect of dose (g) on % adsorption of Al^{3+} over eucalyptus wood waste-derived biochar.

different temperatures (20°C, 40°C, 60°C, and 80°C). As the temperature rises, the equilibrium adsorption capacity rapidly decreases. The decrease in adsorption with increasing temperature may be due to the weakening of the attractive force between the adsorbate and the adsorbent [57].

3.2.5. Effect of pH

Investigating the ideal pH for Al^{3+} adsorption is crucial because the pH of the investigated solution system is crucial for both the state of the adsorbate and the surface chemical characteristics of the adsorbent. It has been studied how well EWB adsorbs Al^{3+} in the pH range of 2.0–6.0. The related adsorption tests were carried out at 25°C and a pH range of 2.0–6.0 in order to assess the impact of pH on the adsorption of Al^{3+} on EWB and to optimise a specific pH for maximum adsorption efficiency.

Fig. 8 clearly illustrates how the variation trends are similar in nature and how the adsorption capacity quickly rises with increasing pH. When the pH was 5.0, the adsorption capacity of activated carbon for Al^{3+} was at its highest, and at pH 6.0, it began to gradually decline. The cause may be due to the high concentration of hydrogen ions in the solution at low pH levels, which results in reduced active adsorption sites due to the competing adsorption of hydrogen ions and Al^{3+} at low pH levels [17,55]. As a result, the Al^{3+} adsorption studies that follow are carried out at a solution pH of 5.0.

3.3. Adsorption kinetics

To further understand the adsorption process, the pseudo-first-order and pseudo-second-order adsorption kinetic models are introduced. The formulas are provided in
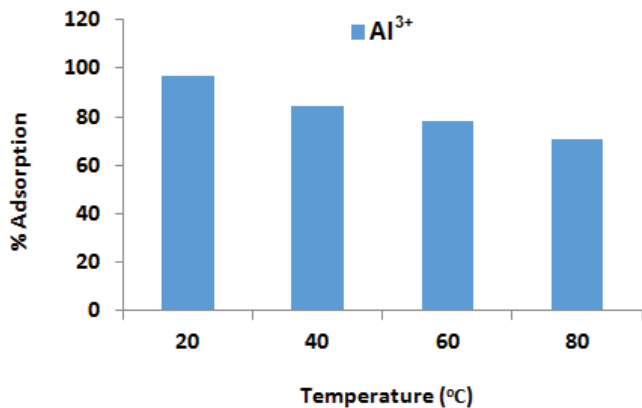
(Table 6). Fig. 9 and Table 6 display the findings. The pseudo-second-order model has a higher R^2 than the pseudo-first-order model for EWB. Furthermore, the adsorption quantities calculated by the pseudo-second-order model are significantly more similar to the experimentally obtained values. Therefore, the pseudo-second-order model is more suitable for describing the adsorption kinetics, which also indicates that chemisorption mainly controls the adsorption of Al^{3+} on EWB.

3.4. Adsorption isotherms

Langmuir and Freundlich adsorption isotherms are utilized to fit the experimental results in order to more thoroughly investigate the interaction mechanism between the EWB and Al^{3+} (Table 6). According to Fig. 10, the adsorption of Al^{3+} by EWB is more compatible with the Langmuir isotherm model because the R^2 of the Langmuir isotherm is
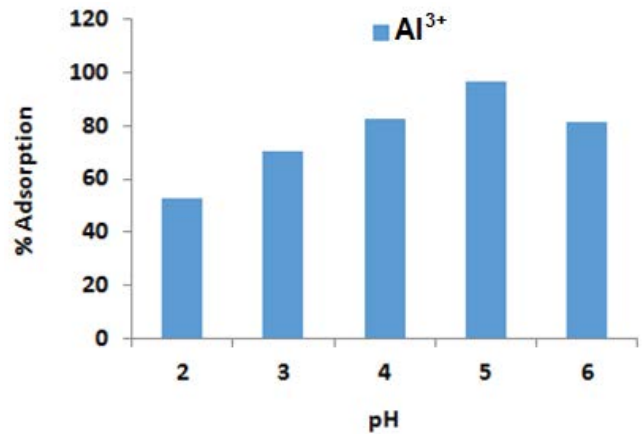
Fig. 8. Effect of pH on % adsorption of Al^{3+} over eucalyptus wood waste-derived biochar.
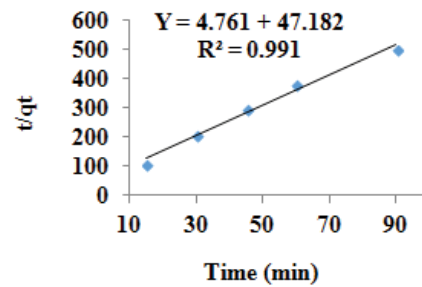
Fig. 9. Pseudo-second-order kinetics for the adsorption of Al^{3+} onto eucalyptus wood waste-derived biochar.

Fig. 7. Effect of temperature on % adsorption of Al^{3+} over eucalyptus wood waste-derived biochar.

Table 6
Pseudo-second-order kinetic and isotherm model parameters for adsorption of Al^{3+} over eucalyptus wood waste-derived biochar

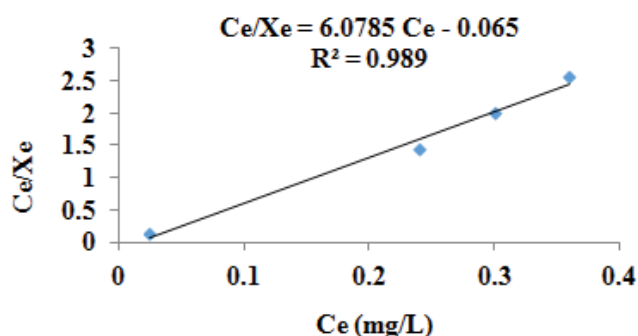| Adsorbents	Pseudo-second-order			Isotherm model		
	K_2 (mg/g·min)	q_e^2 (mg/g)	R^2	q_m (mg/g)	K_1	R^2
Eucalyptus wood waste-derived biochar	0.001	0.210	0.991	0.164	0.395	0.989

Fig. 10. Langmuir isotherms for the adsorption of Al^{3+} onto eucalyptus wood waste-derived biochar.

Table 7
Thermodynamic parameters of eucalyptus wood waste-derived biochar at different temperatures

Temperature (K)	Al^{3+}		
	$\Delta G°$ (kJ/mol)	$\Delta H°$ (kJ/mol)	$\Delta S°$ (kJ/mol)
293	−8.05		
313	−5.61	−38.53	−102.82
333	−4.96		
353	−2.89397		

higher than that of the Freundlich isotherm. It shows that the distribution of active sites on the adsorbent is quite uniform, the adsorbed Al^{3+} molecules dissociate from each other, and the Al^{3+} adsorption on EWB is more consistent with monolayer adsorption.

3.5. Adsorption thermodynamics

To better understand the energy variation during the adsorption process and to make more accurate predictions about the adsorption process, it is helpful to examine the adsorption thermodynamic parameters. Eqs. (8)–(10) can be used to calculate the thermodynamic parameters, as shown in Table 4.

Table 7 displays the relevant variables. A lower temperature is more conducive to the adsorption process, as seen by the negative drop in ΔG, which also shows that the adsorption of Al^{3+} by the EWB is spontaneous. Since EWB has a ΔH value of −38.53, the adsorption process is exothermic. The decrease in randomness at the solid–liquid interface during Al^{3+} adsorption via EWB is shown by the negative ΔS values.

3.6. Comparison of adsorption potential of different adsorbents

Table 8 for Al^{3+} adsorption summarizes the comparative adsorption efficiencies of the adsorbents, especially EWB and various adsorption media. Statistics show that the adsorption efficiency of EWB is higher than any other adsorbent. The increased adsorption capacity used in our investigation, which appears to be responsible for the EWB performance, is driven by the larger surface area.

Table 8
Comparison of different adsorbents used for Al^{3+} adsorption

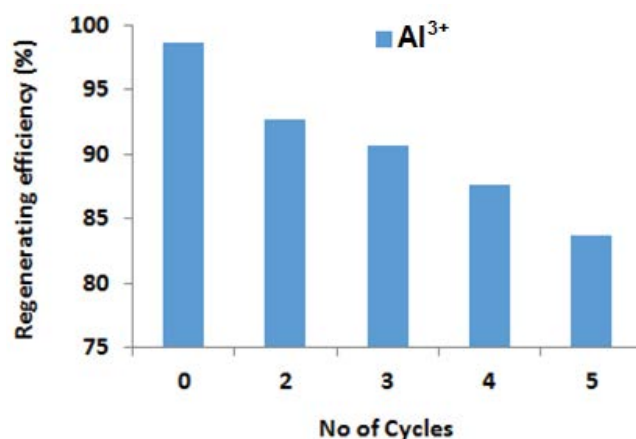|	Adsorption potential (mg/g)	References
Adsorbent	Al^{3+}	
Eucalyptus wood waste-derived biochar	139.20	This article
PAN beads as-prepared	0.25	[58]
BDH activated carbon	0.02	[59]
Date pit	0.31	[59]
AXAD-16 resin	24.3	[60]
201 × 8 anion resin	5.6	[61]
XAD-4	4.4	[62]
IIP-PEI/SiO$_2$	53.5	[63]

Fig. 11. Regenerating efficiency of eucalyptus wood waste-derived biochar.

3.7. Reusability of the EWB

Five adsorption–desorption cycles were used in the reusability research. Shaking adsorption of 0.3 g dried EWB in 100 mL Al^{3+} solution occurred for 90 min (Fig. 11). The adsorbed EWB was then submerged in 0.1 M HCl solution for 1 h of regeneration. The regenerated EWB underwent additional adsorption performance testing after being vacuum dried.

4. Conclusion

Herein, we have provided a simple method for preparing biochar from eucalyptus wood waste. The developed EWB can be severed as an efficient adsorbent to remove Al^{3+} from aqueous solution as well as wastewater. The effective synthesis and microstructure of the EWB were confirmed by a number of characterisation techniques. EWB possess a porous structure and large specific surface area, which provides sufficient active adsorption sites for Al^{3+}. Moreover, the external factors affecting the adsorption performance were fully investigated. The outcomes demonstrated the EWB's superior reusability and high removal efficiency.

The adsorption process is well modelled by the pseudo-second-order and Langmuir models. The findings of this work suggest that EWB is a potential adsorbent with the potential to effectively remove Al^{3+} from aqueous solutions. For future work, we plan to examine the adsorption efficiency of EWB for organic and inorganic pollutants.

References

[1] D. Diaconu, M.M. Nanau, E. Nechifor, O. Nechiforc, R. Doaconu, Aluminum concentration in drinking water from Moldova territory, Romania, Ovidius Univ. Ann. Chem., 20 (2009) 115–118.

[2] R.F. Fard, K. Naddafi, M.S. Hassanvand, M. Khazaei, F. Rahmani, Trends of metals enrichment in deposited particulate matter at semi-arid area of Iran, Environ. Sci. Pollut. Res., 25 (2018) 18737–18751.

[3] M.S. Qaiyum, M.S. Shaharudin, A.I. Syazwan, A. Muhaimin, Health risk assessment after exposure to aluminium in drinking water between two different villages, J. Water Resour. Prot., 3 (2011) 268–274.

[4] M.R. Siti Farizwana, S. Mazrura, A. Zurahanim Fasha, G. Ahmad Rohi, Determination of aluminium and physicochemical parameters in the palm oil estates water supply at Johor, Malaysia, J. Environ. Public Health, 2010 (2010) 615176, doi: 10.1155/2010/615176.

[5] L. Simonsen, H. Johnsen, S.P. Lund, E. Matikainen, U. Midtgård, A. Wennberg, Methodological approach to the evaluation of neurotoxicity data and the classification of neurotoxic chemicals, Scand. J. Work Environ. Health, 20 (1994) 1–12.

[6] M. Gidding, Aluminum, Environmental and Workplace Health Canadian Drinking Water Quality, Canada, 1998.

[7] R. Camarillo, Á. Pérez, P. Cañizares, A. de Lucas, Removal of heavy metal ions by polymer enhanced ultrafiltration: batch process modeling and thermodynamics of complexation reactions, Desalination, 286 (2012) 193–199.

[8] R. Aravindhan, B. Madhan, J.R. Rao, B.U. Nair, T. Ramasami, Bioaccumulation of chromium from tannery wastewater: an approach for chrome recovery and reuse, Environ. Sci. Technol., 38 (2004) 300–306.

[9] J.J. Testa, M.A. Grela, M.I. Litter, Heterogeneous photocatalytic reduction of chromium(VI) over TiO_2 particles in the presence of oxalate: involvement of Cr(V) species, Environ. Sci. Technol., 38 (2004) 1589–1594.

[10] C.A. Kozlowski, W. Walkowiak, Removal of chromium(VI) from aqueous solutions by polymer inclusion membranes, Water Res., 36 (2002) 4870–4876.

[11] V.K. Gupta, A.K. Shrivastava, N. Jain, Biosorption of chromium(VI) from aqueous solutions by green algae *Spirogyra* species, Water Res., 35 (2001) 4079–4085.

[12] H.F. Shaalan, M.H. Sorour, S.R. Tewfik, Simulation and optimization of a membrane system for chromium recovery from tanning wastes, Desalination, 141 (2001) 315–324.

[13] J.C. Seaman, P.M. Bertsch, L. Schwallie, *In-situ* Cr(VI) reduction within coarse-textured, oxide-coated soil and aquifer systems using Fe(II) solutions, Environ. Sci. Technol., 33 (1999) 938–944.

[14] S.K. Srivastava, V.K. Gupta, D. Mohan, Removal of lead and chromium by activated slag—a blast-furnace waste, J. Environ. Eng., 123 (1997) 461–468.

[15] D. Petruzzelli, R. Passino, G. Tiravanti, Ion-exchange process for chromium removal and recovery from tannery wastes, Ind. Eng. Chem. Res., 34 (1995) 2612–2617.

[16] K.L. Shih, J. Lederberg, Chloramine mutagenesis in *Bacillus subtilis*, Science, 192 (1976) 1141–1143.

[17] M. Ilyas, W. Ahmad, H. Khan, I. Ahmad, Application of composite adsorbents prepared from waste PS and PET for removal of Cr and Cu ions from wastewater, Desal. Water Treat., 171 (2019) 144–157.

[18] C.S. Umpierres, P.S. Thue, E.C. Lima, G.S.D. Reis, I.A. de Brum, W.S.D. Alencar, S.L. Dias, G.L. Dotto, Microwave-activated carbons from tucumã (*Astrocaryum aculeatum*) seed for efficient removal of 2-nitrophenol from aqueous solutions, Environ. Technol., 39 (2018) 1173–1187.

[19] A.M.D. Al Ketife, F. Almomani, H. Znad, Sustainable removal of copper from wastewater using chemically treated bio-sorbent: Characterization, mechanism and process kinetics, Environ. Technol. Innovation, 23 (2021) 101555, doi: 10.1016/j.eti.2021.101555.

[20] E.N. Mahmoud, F.Y. Fayed, K.M. Ibrahim, S. Jaafreh, Removal of cadmium, copper, and lead from water using bio-sorbent from treated olive mill solid residue, Environ. Health Insights, 15 (2021), doi: 10.1177/11786302211053176.

[21] M. Tangestani, B. Naeimi, S. Dobaradaran, M. Keshtkar, P. Salehpour, Z. Fouladi, S. Zareipour, F. Sadeghzadeh, Biosorption of fluoride from aqueous solutions by *Rhizopus oryzae*: isotherm and kinetic evaluation, Environ. Prog. Sustainable Energy, 41 (2022) e13725, doi: 10.1002/ep.13725.

[22] K. Rambabu, A. Thanigaivelan, G. Bharath, N. Sivarajasekar, F. Banat, P.L. Show, Biosorption potential of *Phoenix dactylifera* coir wastes for toxic hexavalent chromium sequestration, Chemosphere, 268 (2021) 128809, doi: 10.1016/j.chemosphere.2020.128809.

[23] A.H. Mahvi, S. Dobaradaran, R. Saeedi, M.J. Mohammadi, M. Keshtkar, A. Hosseini, M. Moradi, F.F. Ghasemi, Determination of fluoride biosorption from aqueous solutions using *Ziziphus* leaf as an environmentally friendly cost effective biosorbent, Fluoride, 51 (2018) 220–229.

[24] M. Khorsand, S. Dobaradaran, E. Kouhgardi, Cadmium removal from aqueous solutions using *Moringa oleifera* seed pod as a biosorbent, Desal. Water Treat., 71 (2017) 327–333.

[25] W.S. Chai, W.G. Tan, H.S.H. Munawaroh, V.K. Gupta, S.-H. Ho, P.L. Show, Multifaceted roles of microalgae in the application of wastewater biotreatment: a review, Environ. Pollut., 269 (2021) 116236, doi: 10.1016/j.envpol.2020.116236.

[26] S. Dobaradaran, A.A. Babaei, I. Nabipour, S. Tajbakhsh, S. Noshadi, M. Keshtkar, M. Khorsand, N.M. Esfahani, Determination of fluoride biosorption from aqueous solutions using *Sargassum hystrix* algae, Desal. Water Treat., 63 (2017) 87–95.

[27] S. Dobaradaran, M. Ali Zazuli, M. Keshtkar, S. Noshadi, M. Khorsand, F. Faraji Ghasemi, V. Noroozi Karbasdehi, L. Amiri, F. Soleimani, Biosorption of fluoride from aqueous phase onto *Padina sanctae-crucis* algae: evaluation of biosorption kinetics and isotherms, Desal. Water Treat., 57 (2016) 28405–28416.

[28] M. Agarwa, K. Singh, J. Heavy metal removal from wastewater using various adsorbents: a review, J. Water Reuse Desal., 7 (2017) 387–419.

[29] A.M. Elgarahy, K.Z. Elwakeel, S.H. Mohammad, G.A. Elshoubaky, A critical review of biosorption of dyes, heavy metals and metalloids from wastewater as an efficient and green process, Cleaner Eng. Technol., 4 (2021) 100209, doi: 10.1016/j.clet.2021.100209.

[30] N.M. Alandis, W. Mekhamer, O. Aldayel, J.A.A. Hefne, M. Alam, Adsorptive applications of montmorillonite clay for the removal of Ag(I) and Cu(II) from aqueous medium, J. Chem., 2019 (2019) 7129014, doi: 10.1155/2019/7129014.

[31] M. Keshtkar, S. Dobaradarana, I. Nabipour, A.H. Mahvie, F.F. Ghasemi, Z. Ahmadi, M. Heydari, Isotherm and kinetic studies on fluoride biosorption from aqueous solution by using cuttlebone obtained from the Persian Gulf, Fluoride, 49 (2016) 343–351.

[32] S. Dobaradaran, I. Nabipour, A.H. Mahvi, M. Keshtkar, F. Elmi, F. Amanollahzade, M. Khorsand, Fluoride removal from aqueous solutions using shrimp shell waste as a cheap biosorbent, Fluoride, 47 (2014) 253–257.

[33] C. Vanlalveni, S. Lallianrawna, A. Biswas, M. Selvaraj, B. Changmai, S.L. Rokhum, Green synthesis of silver nanoparticles using plant extracts and their antimicrobial activities: a review of recent literature, RSC Adv., 11 (2021) 2804–2837.

[34] M.R. Awual, M.M. Hasan, A ligand based innovative composite material for selective lead(II) capturing from wastewater, J. Mol. Liq., 294 (2019) 111679, doi: 10.1016/j.molliq.2019.111679.

[35] K.Z. Elwakeel, A.M. Elgarahy, Z.A. Khan, M.S. Almughamisi, A.S. Al-Bogami, Perspectives regarding metal/mineral-incorporating materials for water purification: with special focus on Cr(VI) removal, Mater. Adv., 1 (2020) 1546–1574.

[36] A. Mittal, R. Ahmad, I. Hasan, Iron oxide-impregnated dextrin nanocomposite: synthesis and its application for the biosorption of Cr(VI) ions from aqueous solution, Desal. Water Treat., 57 (2016) 15133–15145.

[37] M.R. Awual, Ring size dependent crown ether based mesoporous adsorbent for high cesium adsorption from wastewater, Chem. Eng. J., 303 (2016) 539–546.

[38] A. Benettayeb, A. Morsli, K.Z. Elwakeel, M.F. Hamza, E. Guibal, Recovery of heavy metal ions using magnetic glycine-modified chitosan—application to aqueous solutions and tailing leachate, Appl. Sci., 11 (2021) 8377, doi: 10.3390/app11188377.

[39] J. Mittal, R. Ahmad, A. Mariyam, V.K. Gupta, A. Mittal, Expeditious and enhanced sequestration of heavy metal ions from aqueous environment by papaya peel carbon: a green and low-cost adsorbent, Desal. Water Treat., 210 (2021) 365–376.

[40] M.R. Awual, T. Yaita, S. Suzuki, H. Shiwaku, Ultimate selenium(IV) monitoring and removal from water using a new class of organic ligand based composite adsorbent, J. Hazard. Mater., 291 (2015) 111–119.

[41] K.Z. Elwakeel, A. Shahat, A.S. Al-Bogami, B. Wijesiri, A. Goonetilleke, The synergistic effect of ultrasound power and magnetite incorporation on the sorption/desorption behavior of Cr(VI) and As(V) oxoanions in an aqueous system, J. Colloid Interface Sci., 569 (2020) 76–88.

[42] R. Ahmad, I. Hasan, A. Mittal, Adsorption of Cr(VI) and Cd(II) on chitosan grafted polyaniline-OMMT nanocomposite: isotherms, kinetics and thermodynamics studies, Desal. Water Treat., 58 (2017) 144–153.

[43] M.R. Awual, T. Yaita, T. Kobayashi, H. Shiwaku, S. Suzuki, Improving cesium removal to clean-up the contaminated water using modified conjugate material, J. Environ. Chem. Eng., 8 (2020) 103684, doi: 10.1016/j.jece.2020.103684.

[44] M.S. Almughamisi, Z.A. Khan, W. Alshitari, K.Z. Elwakeel, Recovery of chromium(VI) oxyanions from aqueous solution using Cu(OH)$_2$ and CuO embedded chitosan adsorbents, J. Polym. Environ., 28 (2020) 47–60.

[45] H. Daraei, A. Mittal, Investigation of adsorption performance of activated carbon prepared from waste tire for the removal of methylene blue dye from wastewater, Desal. Water Treat., 90 (2017) 294–298.

[46] M.R. Awual, Assessing of lead(III) capturing from contaminated wastewater using ligand doped conjugate adsorbent, Chem. Eng. J., 289 (2016) 65–73.

[47] K.Z. Elwakeel, E. Guibal, Potential use of magnetic glycidyl methacrylate resin as a mercury sorbent: from basic study to the application to wastewater treatment, J. Environ. Chem. Eng., 4 (2016) 3632–3645.

[48] S. Soni, P.K. Bajpai, D. Bharti, J. Mittal, C. Arora, Removal of crystal violet from aqueous solution using iron based metal organic framework, Desal. Water Treat., 205 (2020) 386–399.

[49] M.R. Awual, T. Yaita, H. Shiwaku, Design a novel optical adsorbent for simultaneous ultra-trace cerium(III) detection, sorption and recovery, Chem. Eng. J., 228 (2013) 327–335.

[50] M.R. Awual, Solid phase sensitive palladium(II) ions detection and recovery using ligand based efficient conjugate nanomaterials, Chem. Eng. J., 300 (2016) 264–272.

[51] M.R. Awual, A novel facial composite adsorbent for enhanced copper(II) detection and removal from wastewater, Chem. Eng. J., 266 (2015) 368–375.

[52] M.R. Awual, A facile composite material for enhanced cadmium(II) ion capturing from wastewater, J. Environ. Chem. Eng., 7 (2019) 103378, doi: 10.1016/j.jece.2019.103378.

[53] M. Ilyas, W. Ahmad, H. Khan, Utilization of activated carbon derived from waste plastic for decontamination of polycyclic aromatic hydrocarbons laden wastewater, Water Sci. Technol., 84 (2021) 609–631.

[54] M. Ilyas, W. Ahmad, H. Khan, Polycyclic aromatic hydrocarbons removal from vehicle-wash wastewater using activated char, Desal. Water Treat., 236 (2021) 55–68.

[55] M. Ilyas, H. Khan, W. Ahmad, Conversion of waste plastics into carbonaceous adsorbents and their application for wastewater treatment, Int. J. Environ. Anal. Chem., (2022) 1–9, doi: 10.1080/03067319.2022.2062571.

[56] C.P. Dwivedi, J.N. Sahu, C.R. Mohanty, B.R. Mohan, B.C. Meikap, Column performance of granular activated carbon packed bed for Pb(II) removal, J. Hazard. Mater., 156 (2008) 596–603.

[57] J.E. Asuquo, I.S. Udegbunam, E.E. Etim, Effect of temperature on the adsorption of metallic soaps of castor seed oil onto haematite, Int. J. Adv. Res. Chem. Sci., 4 (2017) 40–44.

[58] Z. Aly, A. Graulet, N. Scales, T. Hanley, Removal of aluminium from aqueous solutions using PAN-based adsorbents: characterisation, kinetics, equilibrium and thermodynamic studies, Environ. Sci. Pollut. Res., 21 (2014) 3972–3986.

[59] S.A. Al-Muhtaseb, M.H. El-Naas, S. Abdallah, Removal of aluminum from aqueous solutions by adsorption on date-pit and BDH activated carbons, J. Hazard. Mater., 158 (2008) 300–307.

[60] A. Islam, H. Ahmad, N. Zaidi, S. Yadav, Selective separation of aluminum from biological and environmental samples using glyoxal-bis(2-hydroxyanil) functionalized Amberlite XAD-16 resin: kinetics and equilibrium studies, Ind. Eng. Chem. Res., 52 (2013) 5213–5220.

[61] M. Luo, S. Bi, Solid phase extraction–spectrophotometric determination of dissolved aluminum in soil extracts and ground waters, J. Inorg. Biochem., 97 (2003) 173–178.

[62] J.L. Boudenne, S. Boussetta, C. Brach-Papa, C. Branger, A. Margaillan, F. Théraulaz, Modification of poly(styrene-co-divinylbenzene) resin by grafting on an aluminium selective ligand, Polym. Int., 51 (2002) 1050–1057.

[63] F. An, B. Gao, X. Huang, Y. Zhang, Y. Li, Y. Xu, Z. Zhang, J. Gao, Z, Selectively removal of Al(III) from Pr(III) and Nd(III) rare earth solution using surface imprinted polymer, React. Funct. Polym., 73 (2013) 60–65.